ACS APPLIED MATERIALS & INTERFACES
Research Article
www.acsami.org

Influence of Silver Incorporation on the Structural and Electrical Properties of Diamond-Like Carbon Thin Films

Neeraj Dwivedi,*[,†,‡] Sushil Kumar,*[,†] J. David Carey,[§] R. K. Tripathi,[†] Hitendra K. Malik,[‡] and M. K. Dalai[†]

[†]National Physical Laboratory (CSIR), K.S. Krishnan Road, New Delhi 110 012, India
[‡]Department of Physics, Indian Institute of Technology Delhi, New Delhi 110016, India
[§]Advanced Technology Institute, University of Surrey, Guildford, GU2 7XH, Surrey, United Kingdom

ABSTRACT: A simple approach is proposed for obtaining low threshold field electron emission from large area diamond-like carbon (DLC) thin films by sandwiching either Ag dots or a thin Ag layer between DLC and nitrogen-containing DLC films. The introduction of silver and nitrogen is found to reduce the threshold field for emission to under 6 V/μm representing a near 46% reduction when compared with unmodified films. The reduction in the threshold field is correlated with the morphology, microstructure, interface, and bonding environment of the films. We find modifications to the structure of the DLC films through promotion of metal-induced sp^2 bonding and the introduction of surface asperities, which significantly reduce the value of the threshold field. This can lead to the next-generation, large-area simple and inexpensive field emission devices.

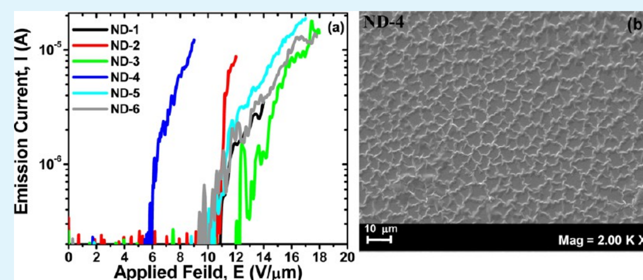

KEYWORDS: *diamond-like carbon, silver, field emission, threshold field, Raman spectroscopy, microscopy*

1. INTRODUCTION

Recently, low-dimensional carbon materials, such as carbon nanotubes (CNTs) and graphene, have shown excellent electronic properties and have opened up the possibility to develop new electronics beyond silicon. CNTs and graphene are both highly conducting materials and have been used for the fabrication of electronic devices, though their large-scale production is still awaited. CNTs, CNT-composites, and graphene all exhibit excellent field emission (FE) characteristics leading to their potential application as X-ray sources for security applications or mobile medical diagnostics or in field emission displays or lighting (FEDs);[1−3] however, their manufacture for large-area electronic applications remains complex. By contrast, other low-dimensional carbon materials, such as diamond-like carbon (DLC) thin films, can be readily produced over large areas and on substrates held at low (room) temperature. These films possess both sp^3- and sp^2-bonded carbon and exhibit tunable mechanical, electrical, and optical properties.[4−15] Here, we focus on the FE characteristics of DLC films and suggest ways to reduce the electric field required to initiate emission by adjusting the sp^2 carbon phase and surface morphology.

Cold electron field emission is the process in which electrons from a cathode are extracted from a surface through quantum tunneling through the surface potential barrier by the application of an electric field. The threshold field (E_T) for emission, an essential material parameter, reflects the onset of emission, and for good field emission devices E_T should be as low as possible. Previous studies of DLC-based field emission devices have shown E_T can be as high as 10−20 V/μm. For example, Ilie et al.[15] have found E_T in the range 21−10 V/μm in amorphous carbon films, whereas Silva et al.[16] have found E_T close to 5 V/μm in nanostructured DLC films having N contents as high as 11 at. % and 15 at. %. Forrest et al.[17] examined the effect of the thickness of hydrogenated DLC (a-C:H) and nitrogenated tetrahedral amorphous carbon (ta-C:N) films on the field emission characteristics of their films and found high values of E_T in a-C:H films which varied between 60 and 10 V/μm, though lower values were found in ta-C:N films. Carey et al.[18−21] explored the effect of self-bias and nitrogen content on electronic properties of a-C:H films and the effect on the value of E_T and found variation of E_T from about 26 to 10 V/μm by changing the negative self-bias. They suggested the importance of the size and concentration of sp^2 clusters on field emission from DLC films and have proposed a description that explains the origin of the low-threshold field based on internal field enhancement and dielectric inhomogeneity of conductive sp^2 clusters embedded in an insulating sp^3 matrix. They further discussed the effect of current annealing and hysteresis on field emission from DLC films by changing the insulating sp^3 phase into conductive sp^2 carbon.[22]

Received: January 24, 2013
Accepted: March 14, 2013
Published: March 14, 2013

 © 2013 American Chemical Society

Despite extensive studies of the FE properties of DLC films, values of E_T remain high especially from films deposited by plasma-enhanced chemical vapor deposition (PECVD). As a consequence, there has been considerable interest in developing ways to reduce the value of E_T by introducing nanostructured surfaces to increase the field enhancement and by doping to change the relative sp^2/sp^3 ratio. Nitrogen inclusion in DLC films is usually accompanied by changes in the sp^2 phase[16] and improvements in transport. For example, Khan et al.[23] used low mass ion implantation to convert sp^3 to sp^2 carbon and reported an improvement in conduction as sp^3 carbon bonding was changed to sp^2 carbon. Ahmed et al.[24] observed a reduction in the value of the threshold field for emission upon silver incorporation in the DLC matrix; metal inclusion can help to promote sp^2 bonding. Other metals such as Li, Cs, Ca, Sr, and Ba have also been incorporated in the DLC matrix to lower E_T value;[25] however, metal incorporation requires a hybrid system involving both sputtering and PECVD units which may result in poisoning of the targets.[26] By contrast, the use of a metal interlayer prior to carbon film growth can be a simple and effective way to reduce the value of E_T of DLC thin films and may also help to change the carbon overlayer from their amorphous to nanostructured phases.[27] Lately, we have reduced the value of E_T of DLC films from 14.8 to 11.4 V/μm by employing a Cu interlayer,[28] through the use of a hybrid sputtering and PECVD system. As a result, we have chosen to study the FE characteristics of DLC films in the presence of silver (both dots and a thin interlayer). Silver was chosen due to its low melting point, high conductivity, and high stability characteristics. We will also explore the effect of nitrogen addition to demonstrate how changes in the sp^2 phase depend on the impurity atom and presence of a metal. We correlate the observed changes in the field emission characteristics with the changes in morphology, microstructure, and bonding environment and also with the interface properties of these films.

2. MATERIALS AND METHODS

2.1. Deposition of DLC and Modified DLC Thin Films. Pure and nitrogen-incorporated DLC thin films were deposited at a base pressure of 10^{-5} Torr on well-cleaned *n*- and *p*-type silicon substrates using a radio frequency (13.56 MHz) PECVD system. The working pressure of acetylene (C_2H_2), argon (Ar), and nitrogen (N_2) was kept at 2.4×10^{-3} Torr, and a fixed self-bias of −135 V is used for the deposition of all the films. A pure DLC film (sample ND-1) was grown at a working pressure of 2.4×10^{-3} Torr, obtained by feeding C_2H_2 gas to change the pressure to 7.5×10^{-4} Torr and then Ar gas to change the pressure to 2.4×10^{-3} Torr. A nitrogen-containing DLC film (DLC:N, sample ND-2) was deposited at a working pressure of 2.4×10^{-3} Torr obtained by first feeding C_2H_2 gas and then N_2 gas. Similar DLC and DLC:N films were also produced on Ag dots as shown in Figure 1. First, bare Si substrates (Figure 1a) are taken, and then Ag dots (Figure 1b) are deposited over them with the help of a mask using thermal evaporation. The diameter of each Ag dot is found to be around 500 μm, and the separation between the edges of the dots is ∼500 μm. Subsequent to Ag deposition, DLC and DLC:N layers are grown on the Ag dots (Figure 1c). Sample ND-3 is obtained when a DLC layer is deposited over the Ag dots, and sample ND-4 is obtained when a DLC:N film is deposited over the Ag dots. The samples show the formation of peaks and valleys over the surface (Figure 1d). Owing to a sufficient separation between the Ag dots, two different regions are formed when the DLC or DLC:N layers are grown. One region is located between the Ag dots and possesses a configuration of Si/DLC or Si/DLC:N (called the valley region), and the other region corresponds to a configuration of Si/Ag dots/DLC or Si/Ag dots/DLC:N (called the peak region). Besides using Ag dots, Ag/DLC and Ag/DLC:N bilayers are also deposited for which the Ag interlayer is deposited on the Si substrates using thermal evaporation followed by the deposition of DLC and DLC:N layers over them. When the DLC (DLC:N) film is deposited on a continuous Ag layer, sample ND-5 (sample ND-6) is obtained.

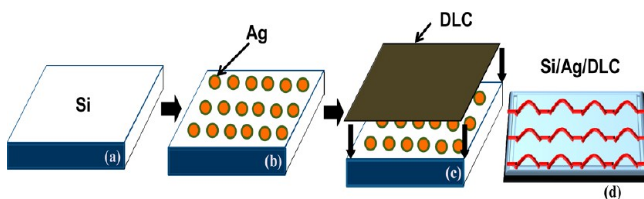

Figure 1. (a)−(d) Schematic representation of deposition of Ag dots containing DLC films.

2.2. Characterization Methods Employed. All the films are characterized for their morphological and structural properties by scanning electron microscopy (SEM) (JEOL, JSM-35), atomic force microscopy (AFM) (Veeco V), and micro Raman spectroscopy (Renishaw inVia Reflex micro Raman spectrometer attached to an air-cooled argon ion laser). Compositional analysis was carried out using time-of-flight secondary ion mass spectroscopy (TOF-SIMS) (TOF-SIMS 5 of ION-TOF GmBH, Germany) and energy-dispersive X-ray analysis (EDAX). The field emission characteristics were examined using a Keithley software controlled field emission measurement unit (Keithley 2410). The thickness of the films was determined using a Taylor-Hobson Talystep and found to be about 160 and 140 nm in DLC (ND-1) and DLC:N (ND-2) films, respectively. The thickness of either Ag dots or the Ag layer is found to be about 55 nm. For micro Raman measurements, 514 nm was used for the excitation source. ToF-SIMS measurements were performed under ultrahigh vacuum conditions with a pressure of 3.75×10^{-10} Torr. Pulsed primary ions from a 25 keV Bi liquid-metal ion gun (LMIG) were used to bombard the sample surface to create secondary ions. The primary ion dose density was approximately 10^{14} ions cm^{-2} for all investigated samples. The sputtering was carried out by using a 500 eV O_2 source to remove the first few layers from the sample surface. The sputtering and the analysis area were kept at 200 × 200 μm^2 and 70 × 70 μm^2, respectively, for all the samples investigated. The overall depth resolution is better than 1 nm. The field emission measurements were carried out at a base pressure of 10^{-7} Torr using a Keithley high voltage source. The sample was placed at the cathode, and an ITO-coated glass slide was used as the anode. Only samples deposited on *n*-type Si were used for field emission characterization.

3. RESULTS AND DISCUSSION

Figures 2a and 2b show the SEM images of the DLC and DLC:N films (samples ND-1 and ND-2) and show the formation of a smooth, textureless surface, a characteristic of amorphous carbon thin films. However, when DLC and DLC:N films are grown over the Ag dots on Si, nano- and microstructures are realized in the resultant Ag dot/DLC (sample ND-3) and Ag dot/DLC:N (sample ND-4) films. Figure 2c shows a larger area SEM image of a DLC film deposited on Ag dots (sample ND-3), and Figure 2d shows a micrograph of sample ND-3 captured from the valley region located between the Ag dots with the corners of the dots visible. This central region is found to be amorphous in nature which is consistent with the structure of sample ND-1. However, the region possessing a Si/Ag dot/DLC configuration (peak region) reveals a change in the morphology, and the formation of small carbon nanostructures is found (Figure 2e). When a DLC:N film is grown over the Ag dots (Ag dot/DLC:N film, sample ND-4), the same two types of regions are

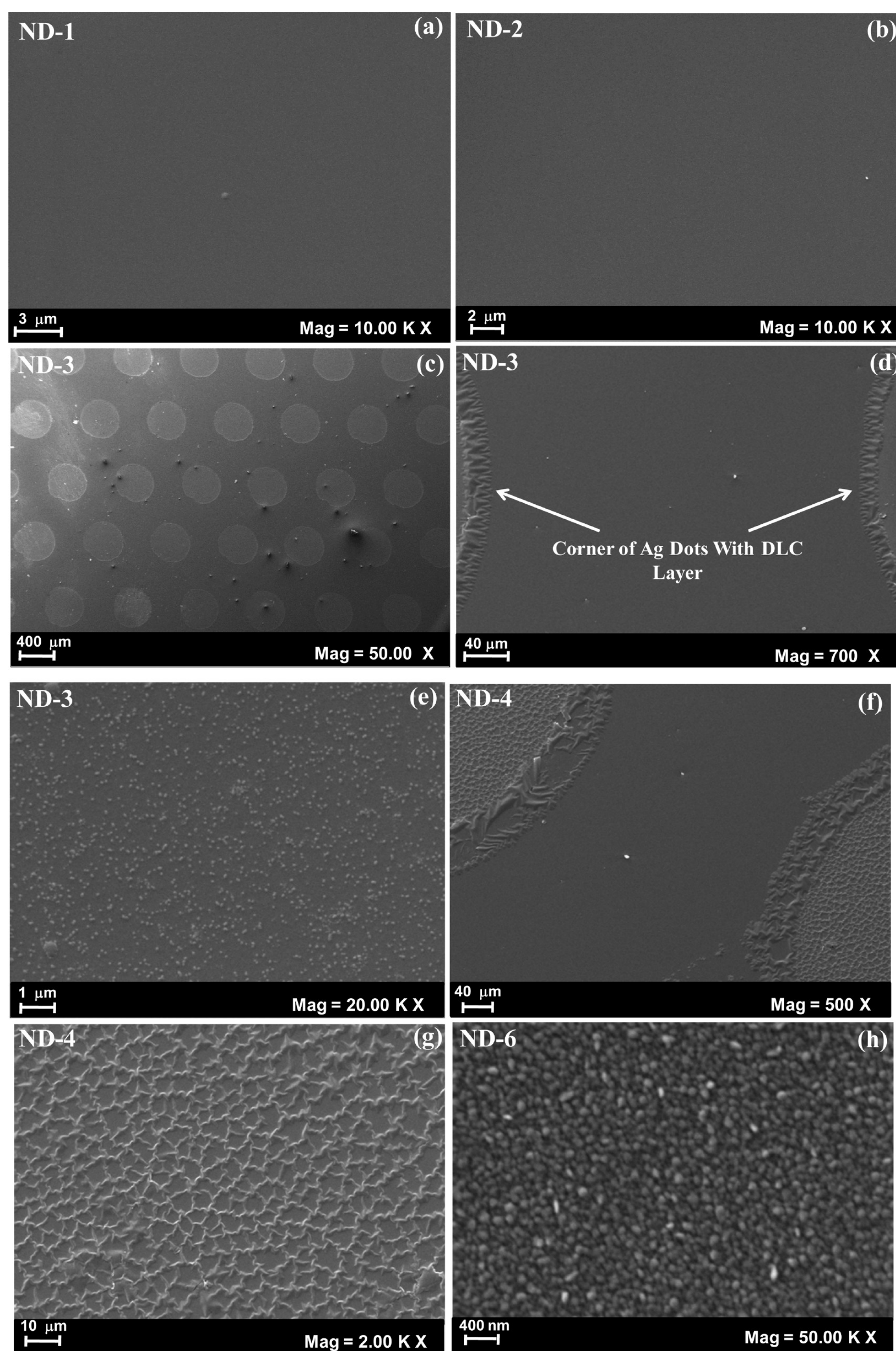

Figure 2. SEM images of samples (a) ND-1, (b) ND-2, (c) ND-3, and (d) ND-3 with a view of the dots in the corner, (e) ND-3 from a peak region, (f) ND-4 with a view of the dots in corner, (g) ND-4 from a peak region, and (h) sample ND-6.

found. The valley region (Figure 2f) is found to be smooth in nature; however, the peak region shows the formation of a different microstructured morphology (Figure 2g). In contrast to the peak region of sample ND-3, here the formation of a chain-like structure is observed. The analysis of samples ND-3 and ND-4 infers that the Ag dots help to change the amorphous structure of the carbon film, observed in samples ND-1 and ND-2, into micro- and nanostructures of carbon. The SEM analysis of DLC:N film grown over the thin Ag layer (configuration Si/Ag layer/DLC:N, sample ND-6) was also conducted and shown in Figure 2h. This sample reveals the formation of well-organized, uniform, and highly dense spherical carbon nanostructures. The average size of carbon nanoparticles in sample ND-6 is found to be between 70 and 80 nm. As metal and nitrogen both help increase the graphite-like sp^2 bonding, it is expected that such micro- and nanostructures have a higher sp^2 carbon content, which is confirmed by micro-Raman analysis (discussed later).

Atomic force microscopy (AFM) analysis has been performed to investigate the morphology and roughness of the DLC and modified DLC films. Figure 3a shows an AFM 3D micrograph of sample ND-1, which clearly reveals a mirror

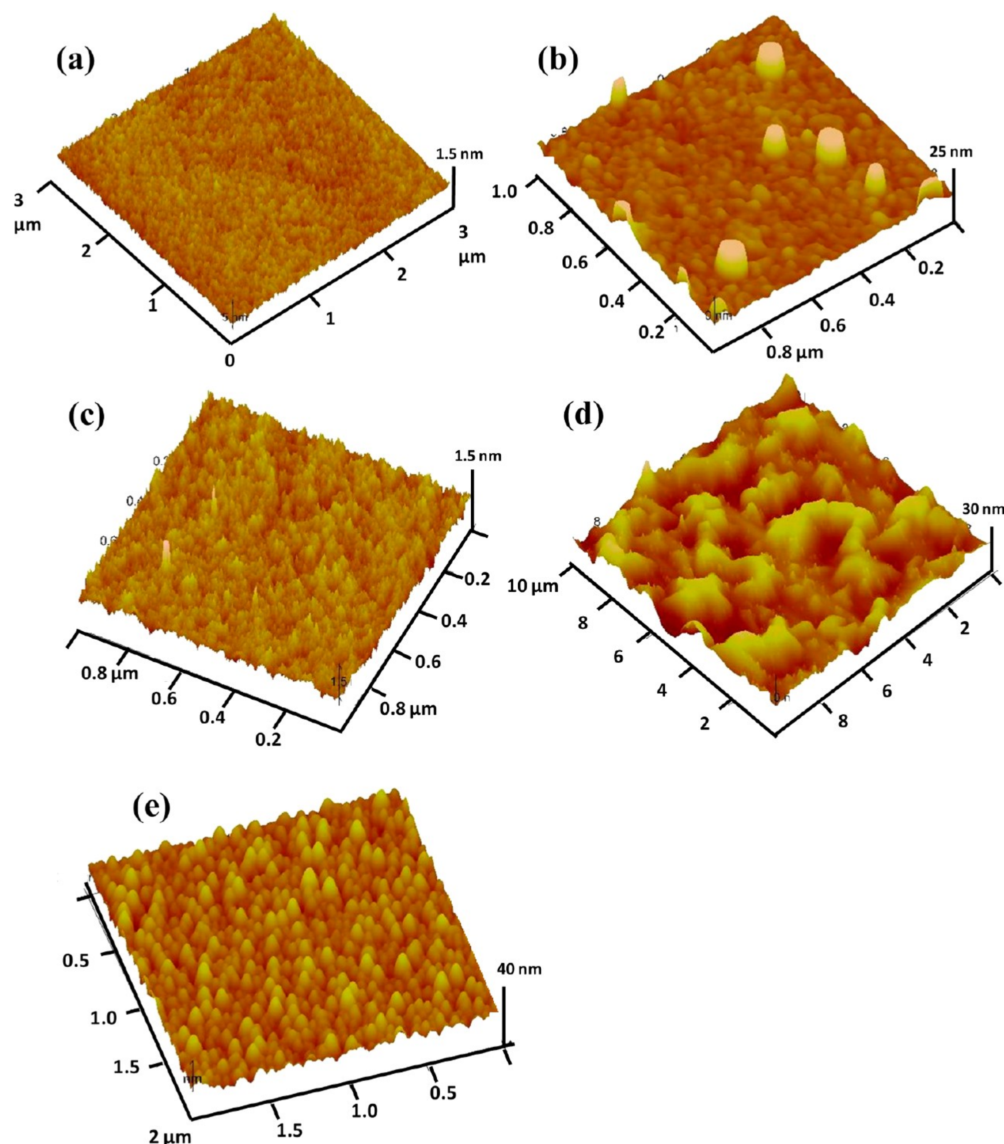

Figure 3. AFM images of samples (a) ND-1, (b) ND-3 from the peak region, (c) ND-3 from the valley region, (d) ND-3 after field emission, and (e) ND-6.

smooth surface, in agreement with the SEM micrograph of the sample ND-1. AFM measurements of sample ND-3 are taken from the peak region (Figure 3b) and valley region (Figure 3c). Here, the DLC layer grown over the Ag dot (peak region) clearly reveals the formation of nanostructures, whereas the area containing the configuration of Si/DLC (valley region) located between the Ag dots is found to be mirror smooth. Figure 3d is the AFM 3D micrograph of the sample ND-3 taken after the FE measurement and reveals structural changes (discussed later) of the surface. The AFM micrograph of the sample ND-6 has also been captured (Figure 3e) and reveals a uniform and high density distribution of carbon nanoparticles on the surface. Hence, it is concluded that both Ag dots and the Ag layer help in the formation of a carbon nanostructured surface. AFM has also been used for surface roughness analysis. The root-mean-square roughness (R_q) of sample ND-1 is found to be 0.12 nm, justifying its mirror smooth description. In the case of the sample ND-3, we have measured R_q from three different regions: in the valley region a value of 0.16 nm is found which increases to 1.5 nm in the peak region owing to the introduction of metallic Ag dots below the DLC layer. The value of R_q in the conditioned area, post field emission testing, is found to be larger at 64 nm. Finally, in sample ND-6 having DLC:N film on the Ag layer, the roughness is found to be 4.8 nm. Since metal films are rougher than the DLC and DLC:N films, the roughness analysis implies that the introduction of Ag (dots or layers) increases the overall roughness of the surface of the film. The grain size of the sample ND-6 is also estimated by AFM, and it is found to be about 80 nm, which agrees well with the SEM analysis.

TOF-SIMS measurements were carried out to investigate the constituents of the films as well as to study the diffusion of atoms into the Si substrate. The depth profiles for samples ND-1 and ND-2 are presented in Figures 4a and 4b, respectively. These figures clearly reveal the diffusion of C, H, and N atoms into the Si substrate. However, among the two samples, the diffusion of C and H atoms into Si is found to be higher in sample ND-1. Among H and C atoms, H diffuses deeper owing to its lower atomic mass. Examination of the depth profile of the other samples suggests that the introduction of nitrogen has

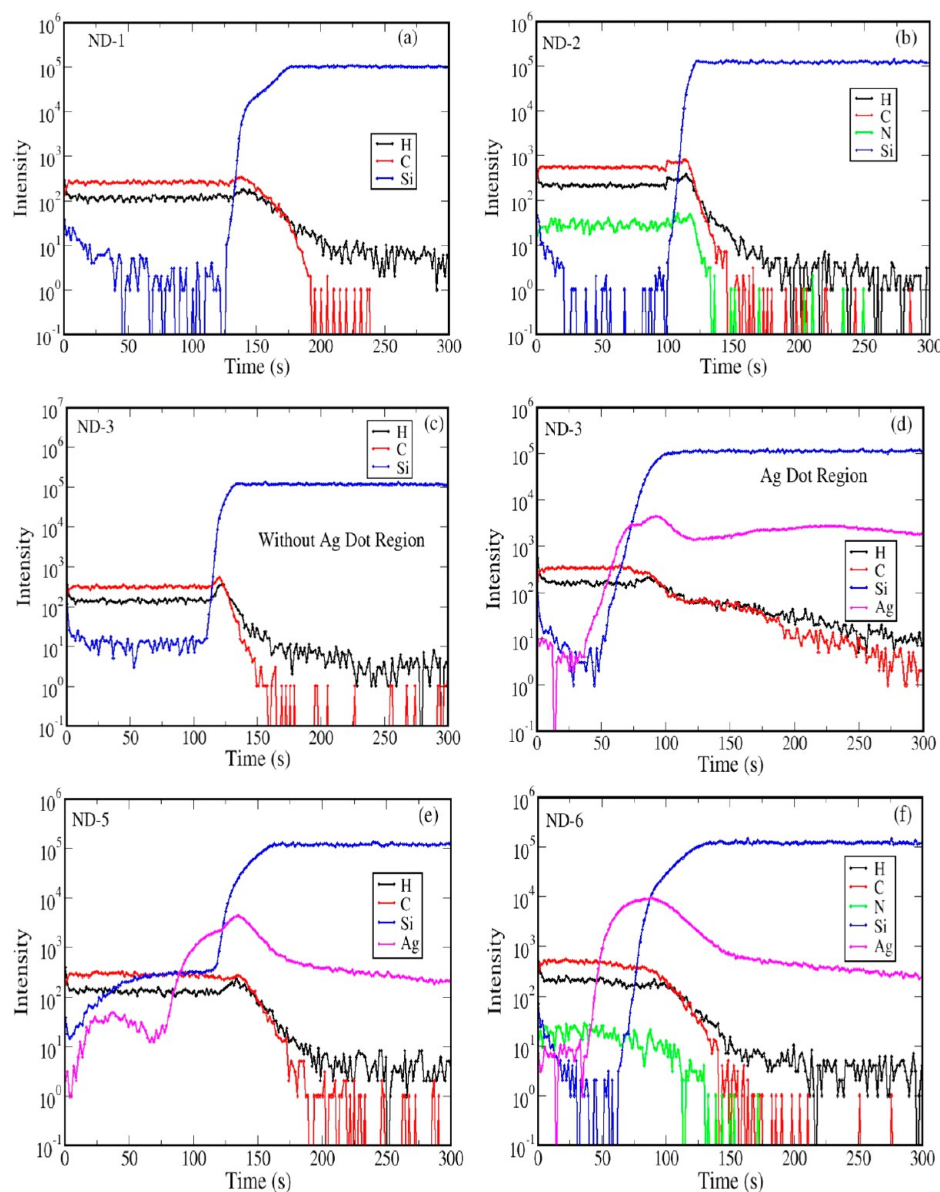

Figure 4. TOF-SIMS depth profiles of samples (a) ND-1, (b) ND-2, (c) ND-3 from the valley region, (d) ND-3 from the peak region, (e) ND-5, and (f) ND-6.

reduced the diffusion of C and H into Si. A consequence of this may be to reduce the interfacial mismatch and interfacial stress and help to improve the adhesion of film to the substrate. Depth profiles of silver-modified DLC and DLC:N films are also recorded for samples ND-3, ND-5, and ND-6. The depth profile of sample ND-3 is recorded both over and away from the silver region. The depth profile of the valley region, where the DLC layer is only over the substrate Si (no Ag dot region), is presented in Figure 4c. The profile of the valley region is similar to the depth profile of sample ND-1 (Figure 4a) and exhibits significant diffusion of C and H atoms into the substrate. The depth profile of the peak region is presented in Figure 4d and reveals that all the constituents Ag, C, and H of this region diffuse into the substrate. The depth profiles for samples ND-5 and ND-6 are presented in Figures 4e–4f. Here, it can be seen that the diffusion of C and H in sample ND-5 is found to be comparable to that of sample ND-1. The diffusion of C and H is further reduced in sample ND-6 due to nitrogen introduction. It can be seen that comparing samples ND-5 and ND-6 the diffusion of Ag into Si is lower in sample ND-6, which may be due to the presence of nitrogen in this sample. The analysis of the TOF-SIMS results reveals the presence of all constituents of the samples and a reduction of C atom diffusion into the substrate due to nitrogen, Ag dots, or Ag interlayer addition. Finally, the approximate percentage of nitrogen in sample ND-2 is calculated by taking the average intensity ratios. The nitrogen content in a sample ND-2 is found to be about 5 at. %. The estimated nitrogen content by TOF-SIMS agrees well with the nitrogen content as estimated by EDAX which is estimated to be about 4.7 at. %.

Raman spectroscopy is found to be one of the most important nondestructive characterization tools for low-dimensional carbon nanomaterials and is able to probe the sp^2 and sp^3 carbon phases separately. The DLC and modified DLC films contain diamond-like sp^3 and graphite-like sp^2 bonding. The room-temperature electronic band gap of 100% crystalline sp^3-bonded diamond is around 5.5 eV, whereas 100% sp^2-bonded graphite has a zero band gap as the $\pi-\pi^*$ bands overlap. In the

case of amorphous carbon films, visible Raman spectroscopy effectively probes the sp^2 phase. Tamor and Vassell,[29] Weiler et al.,[30] Ferrari and Robertson,[31] Ferrari et al.,[32] and Rodil et al.[33] have all widely employed micro Raman technique for probing the microstructure of amorphous carbon thin films. Usually, visible Raman spectra of DLC films exhibit two important bands, namely, the D (disorder) band near 1350 cm^{-1} and the G band near 1550 cm^{-1}. The D band is associated with the A_{1g} breathing mode of phonons near the zone boundary and appears in the presence of disorder; this mode is absent in perfect or crystalline graphite. The G band is the E_{2g} stretching mode and occurs because of in-plane displacement of sp^2 carbon atoms against in-plane restoring forces.[31−33] The Raman spectra of various DLC and modified DLC films, in the range 1000−2000 cm^{-1}, are depicted in Figure 5a−5e. The

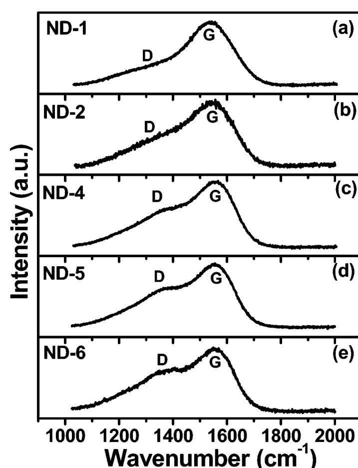

Figure 5. Visible Raman spectra of samples (a) ND-1, (b) ND-2, (c) ND-4, (d), ND-5, and (e) ND-6.

Raman spectrum of each sample reveals the presence of both the D and G peaks. The introduction of nitrogen and Ag (either dots or layer) results in a shifting of the D and G peak positions and a change in the I_D/I_G ratio. To examine the exact D and G peak positions and their I_D/I_G ratios, the Raman spectra were fitted with two Gaussian functions. The variation of the evaluated G peak position and I_D/I_G ratio for different samples is shown in Figures 6a and 6b, respectively. The G peak position and I_D/I_G ratio of sample ND-1 are found to be 1549 cm^{-1} and 0.41, respectively, which increases to 1560 cm^{-1} and 0.69 (sample ND-2); to 1569 cm^{-1} and 0.85 (sample ND-4); to 1568 cm^{-1} and 0.9 (sample ND-5); and to 1569 cm^{-1} and 1.0, respectively (sample ND-6). The increased position of the G peak and the I_D/I_G ratio in nitrogen, Ag dot, and Ag layer modified DLC films are attributed to an increase in sp^2 bonding.

The emission current−applied field (I−E) curves of the films are shown in Figure 7a. Before recording the final FE curves, electrical conditioning was performed until the emission current became stable. The value of the threshold field (E_T) is defined at a current of ∼3 × 10^{-7} A. The DLC film (sample ND-1) shows an E_T of around 11 and about 10.8 V/μm in DLC:N film (sample ND-2). In the DLC/Ag dot film (sample ND-3), E_T is 12.7 V/μm but is significantly reduced to 5.9 V/μm in DLC:N/Ag dot film (sample ND-4). The values of E_T from the DLC/Ag film (sample ND-5) and DLC:N/Ag film (sample ND-6) are found to be 10.4 and 10.1 V/μm,

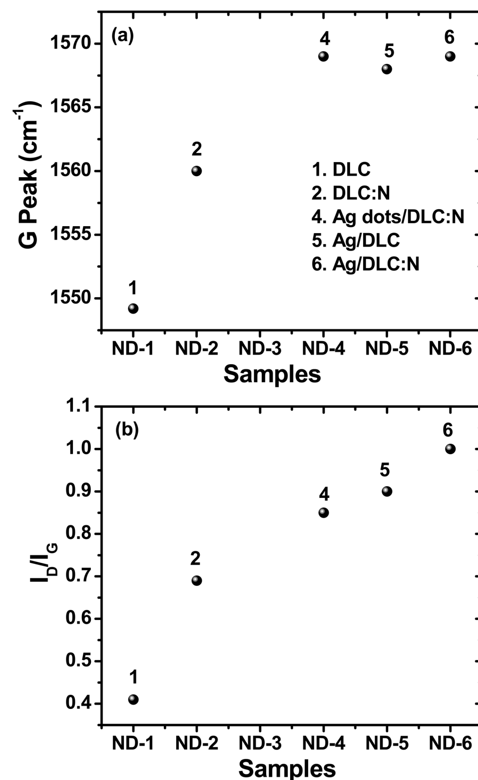

Figure 6. Variations of (a) G peak position and (b) I_D/I_G ratio for various ND samples.

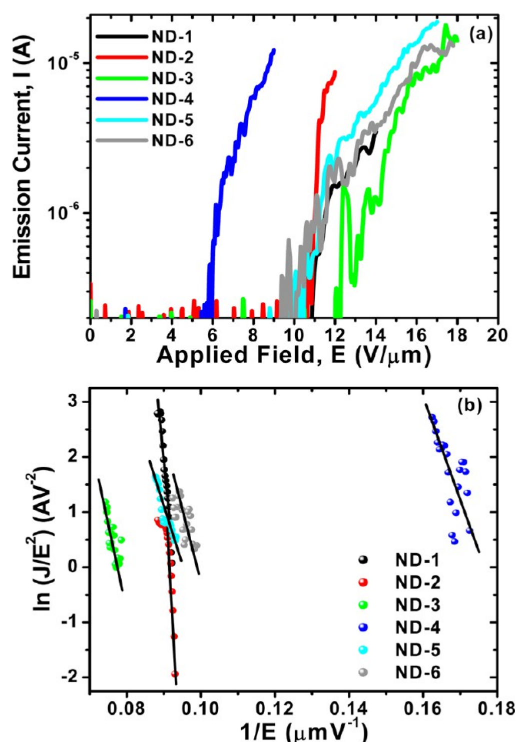

Figure 7. (a) Field emission I−E characteristics and (b) their fitting to the Fowler−Nordheim model for various ND samples.

respectively. To avoid the possibility of field emission from the Ag dots and Ag layer themselves, FE measurements on samples with either Ag dots or Ag layer deposited on an n-Si substrate (without DLC and DLC:N film deposition over

them) were also conducted. Up to a maximum field of 20 V/μm, no emission was recorded, which confirms that the emission of the electrons occurs through carbon-based overlayer structures with the Ag dots and Ag layers helping in the formation of the micro- and nanostructure. The electron emission characteristics of the samples can be fitted (Figure 7b) to the simplified Fowler–Nordheim (F–N) equation

$$J = \frac{a(\beta E)^2}{\phi} \exp\left(\frac{b\phi^{3/2}}{\beta E}\right) \quad (1)$$

where J is the current density; Φ is taken as the barrier height to emission; E is the applied electric field; β is the field enhancement factor; and a and b are constants with values of 1.56×10^{-6} A eV V^{-2} and 6.83×10^{7} V eV$^{-3/2}$ cm^{-1}, respectively. A good fit to the F–N emission mechanism suggests emission of electrons is via tunneling through an approximately triangular front surface potential barrier.

The threshold fields for samples ND-1, ND-2, ND-5, and ND-6 are all similar (10–11 V/μm), whereas sample ND-4 has a much lower threshold field (5.9 V/μm). Samples ND-1 and ND-2 both possess mirror smooth surfaces, though the latter has about 5 at. % N present. Sample ND-3 has some surface roughness in the region with the Ag dots but has a similar flat finish elsewhere. Sample ND-4 has both Ag dots and a textured surface finish, and sample ND-6 has a high concentration of closely spaced spherical surface asperities. In relation to the emission from sample ND-6 it is highly likely that the field lines from the anode terminate at the tips of the asperities, and it is from here that the emission originates. For the other samples it is worth recalling that field emission from DLC films depends on the electronic properties of the films with two generic types of emission mechanisms possible. In general samples grown at low self-bias possess a low defect (electron spin resonance) density[19] as well as low conductivity with a high H content (and high C–H sp^3 content) and are sometimes referred to as polymer-like amorphous carbon (PAC) films.[20] In such films the electron emission is controlled by the properties of the film/substrate contact. Films grown at higher self-biases, such as those in this study, have a higher sp^2 content and a higher conductivity[21] with sp^2 clusters embedded in the insulating sp^3 matrix. The field lines from the anode terminate on the more conductive elements (sp^2 carbon) within the film and give rise to a dielectric inhomogeneity,[20] which helps to increase the field enhancement factor and reduce E_T. As a consequence the electron emission properties of mirror smooth films are determined by the concentration and size of the sp^2 clusters in the film and the properties of the front surface potential barrier. In the DLC films grown here, a so-called front surface controlled emission of electrons is the most probable emission mechanism with the replacement of emitted electrons not limited by transport through the film. The addition of the N helps to increase the size of the clusters (as evidenced by the small change in the G peak position) of sample ND-2 compared to sample ND-1 but without changing significantly the sp^2 concentration or surface morphology; hence, the threshold fields are similar. A higher concentration of N atoms would be needed to affect the surface morphology.

Samples ND-4, -5, and -6 have a similar Raman G peak position, though sample ND-4 has the lowest threshold field. In this case the electron emission is determined by the surface properties (asperities or texture) of the sample. From Figure 2g and Figure 2h samples ND-4 and ND-6 exhibit a high degree of texturing though the key difference which explains the higher threshold field in sample ND-6 is the closeness of the emitting sites. This closeness of the emitters gives rise to a proximity electrostatic screening[34] of the emitters and reduces the electric field experienced at the tip of the emitters. As a result a higher applied field is required even though the Raman spectra suggest similar electronic properties of the film. Finally, we note that the value of E_T for sample ND-3 is the highest at 12.7 V/μm, over twice that of sample ND-4. We repeated the field emission measurements of (new) samples of ND-3 and ND-4 and found the value of E_T to be 12.6 and 5.8 V/μm, respectively, similar to that found previously. The AFM analysis of sample ND-3, post emission, showed some damage with an rms roughness of 63 nm suggesting some form of dielectric breakdown was present in this sample. Our study shows that the choice of a low incorporation of N atoms (<5 at. %) coupled with the different structures of Ag (dots or layers) can result in very different electronic and structural properties which in turn control the field-induced tunneling of electrons. In this study we have been able to distinguish between electron emissions controlled simply by the internal sp^2 phase of the films from emission controlled by surface texturing. The addition of a small amount of N was insufficient alone to lower the threshold field, and the presence of Ag alone was not enough to adjust the surface morphology; it was only the combination of both that reduced the threshold field to less than 6 V/μm.

4. CONCLUSIONS

A variety of DLC and modified DLC films were deposited using the rf-PECVD technique and studied for their structural, compositional, interface, and field emission properties. The addition of Ag dots and Ag interlayers in the DLC and DLC:N films changes their bulk amorphous to micro- and nanostructured morphologies and enhances the sp^2 bonding and reduces the diffusion of C into Si. This suggests that low threshold field emission can be achieved from DLC films by the inclusion of Ag, and N is sufficient to change the sp^2 phase in the films. Among various samples, the lowest threshold field (5.9 V/μm) during the electron emission is encountered in the sample ND-4 owing to the presence of a low concentration of nitrogen and with Ag dots which changed the morphology to a textured surface. Finally, owing to excellent field emission properties, these modified DLC films can be potential candidates for next generation, inexpensive, and large-area field emission devices.

■ AUTHOR INFORMATION

Corresponding Author

*E-mail: neerajdwivedi6@gmail.com (N. D.); skumar@nplindia.org (S.K).

Notes

The authors declare no competing financial interest.

■ ACKNOWLEDGMENTS

Authors are grateful to the Director, National Physical Laboratory, New Delhi (India), for his kind support. Authors wish to thank Mr. Ishpal, Ms. Kalpana Lodhi, Mr. Sandeep, Mr. Jai, Ms. Geetanjali Sehgal, Dr. O. S. Panwar, and Mr. K. N. Sood for their help. ND acknowledges CSIR, Govt. of India, and RKT acknowledges MNRE Govt. of India for providing financial support through SRF and JRF fellowships, respectively.

REFERENCES

(1) Talapatra, S.; Kar, S.; Pal, S. K.; Vajtai, R.; Cl, L.; Victor, P.; Shaijumon, M. M.; Kaur, S.; Nalamasu, O.; Ajayan, P. M. *Nature Nanotechnol.* **2006**, *1*, 112−116.

(2) Connolly, T.; Smith, R. C.; Hernandez, Y.; Gun'ko, Y.; Coleman, J. N.; Carey, J. D. *Small* **2009**, *5*, 826−831.

(3) Varshney, D.; Rao, C. V.; Guinel, M. J. F.; Ishikawa, Y.; Weiner, B. R.; Morell, G. *J. Appl. Phys.* **2011**, *110*, 044324.

(4) Carey, J. D. *Phil. Trans. R. Soc. London A* **2003**, *361*, 2891−2907.

(5) Dwivedi, N.; Kumar, S.; Malik, H. K. *J. Appl. Phys.* **2012**, *112*, 023518.

(6) Erdemir, A.; Donnet, C. *J. Phys. D: Appl. Phys.* **2006**, *39*, 311.

(7) Dwivedi, N.; Kumar, S.; Tripathi, R. K.; Carey, J. D.; Malik, H. K.; Dalai, M. K. *ACS Appl. Mater. Interfaces* **2012**, *4*, 5309−5316.

(8) Dwivedi, N.; Kumar, S.; Rauthan, C. M. S.; Panwar, O. S. *Plasma Process. Polym.* **2011**, *8*, 100−107.

(9) Dwivedi, N.; Kumar, S.; Malik, H. K. *ACS Appl. Mater. Interfaces* **2011**, *3*, 4268−4278.

(10) Tordjman, M.; Bolker, A.; Saguy, C.; Baskin, E.; Bruno, P.; Gruen, D. M.; Kalish, R. *Adv. Funct. Mater.* **2012**, *22*, 1827−1834.

(11) May, P. W.; Hohn, S.; Ashfold, M. N. R.; Wang, W. N.; Fox, N. A.; Davis, T. J.; Steeds, J. W. *J. Appl. Phys.* **1998**, *84*, 1618−1625.

(12) Silva, S. R. P.; Carey, J. D. *Diamond Relat. Mater.* **2003**, *12*, 151−158.

(13) Varshney, D.; Makarov, V. I.; Saxena, P.; Berrios, A. G.; Scott, J. F.; Weiner, B. R.; Morell, G. *Nanotechnology* **2010**, *21*, 285301.

(14) Dwivedi, N.; Kumar, S.; Carey, J. D.; Malik, H. K.; Govind. *J. Appl. Phys.* **2012**, *112*, 113706.

(15) llie, A.; Ferrari, A. C.; Yagi, T.; Rodil, S. E.; Robertson, J.; Barborini, E.; Milani, P. *J. Appl. Phys.* **2001**, *90*, 2024−2032.

(16) Silva, S. R. P.; Amaratunga, G. A. J.; Barnes, J. R. *Appl. Phys. Lett.* **1997**, *71*, 1477−1479.

(17) Forrest, R. D.; Burden, A. P.; Silva, S. R. P.; Cheah, L. K.; Shi, X. *Appl. Phys. Lett.* **1998**, *25*, 3784−3786.

(18) Carey, J. D.; Forrest, R. D.; Silva, S. R. P. *Appl. Phys. Lett.* **2001**, *78*, 2339−2341.

(19) Collins, M.; Barklie, R. C.; Anguita, J. V.; Carey, J. D.; Silva, S. R. P. *Diamond Relat. Mater.* **2000**, *9*, 781−785.

(20) Silva, S. R. P.; Carey, J. D.; Guo, X.; Tsang, W. M.; Poa, C. H. P. *Thin Solid Films* **2005**, *482*, 79−85.

(21) Carey, J. D.; Smith, R. C.; Silva, S. R. P. *J. Mater. Sci.: Mater. Electron.* **2006**, *17*, 405−412.

(22) Carey, J. D.; Silva, S. R. P. *Appl. Phys. Lett.* **2001**, *78*, 347−349.

(23) Khan, R. U. A.; Carey, J. D.; Silva, S. R. P. *Phys. Rev. B* **2001**, *63*, 121201.

(24) Ahmed, S. F.; Moon, M. W.; Lee, K. W. R. *Appl. Phys. Lett.* **2008**, *92*, 193502.

(25) Deguchi, M.; Taomoto, A. *Vacuum* **2010**, *84*, 438−443.

(26) Pauleau, Y.; Theiry, F.; Barna, P. B.; Misjak, F.; Kovacs, A.; Dub, S. N.; Uglov, V. V.; Kuleshov, A. K. *Rev. Adv. Mater. Sci.* **2004**, *6*, 140−149.

(27) Dwivedi, N.; Kumar, S.; Malik, H. K. *J. Appl. Phys.* **2012**, *111*, 014908.

(28) Dwivedi, N.; Kumar, S.; Tripathi, R. K.; Malik, H. K.; Panwar, O. S. *Appl. Phys. A: Mater. Sci. Process.* **2011**, *105*, 417−425.

(29) Tamor, M. A.; Vassell, W. C. *J. Appl. Phys.* **1994**, *76*, 3823.

(30) Weiler, M.; Sattel, S.; Giessen, T.; Jung, K.; Ehrhardt, H.; Veerasamy, V. S.; Robertson, J. *Phys. Rev. B* **1996**, *53*, 1594.

(31) Ferrari, A. C.; Robertson, J. *Philos. Trans. R. Soc. London A* **2004**, *362*, 2477−2512.

(32) Ferrari, A. C.; Rodil, S. E.; Robertson, J. *Phys. Rev. B* **2003**, *67*, 155306.

(33) Rodil, S. E.; Ferrari, A. C.; Robertson, J.; Milne, W. I. *J. Appl. Phys.* **2001**, *89*, 5425−5430.

(34) Nilsson, L.; Groening, O.; Emmenegger, C.; Kuettel, O.; Schaller, E.; Schlapbach, L.; Kind, H.; Bonard, J.-M.; Kern, K. *Appl. Phys. Lett.* **2000**, *76*, 2071−2073.